

# Coherent structures and turbulence in two-dimensional hydrodynamics

Stefano Ugliano<sup>1</sup>

<sup>1</sup>EMMCS student (M1) at University of Warwick

The phenomenon of inverse cascade of energy is a peculiarity of two-dimensional turbulence caused by a nonlinear coupling between different scales of motion in the Navier-Stokes equation. The coherent structures originated by this process are known to have a certain velocity profile  $V \propto r^\alpha$  with  $\alpha = -\frac{1}{4}$ : a numerical simulation of turbulence via forced Navier-Stokes equation seems to contradict this hypothesis, yielding to a different question concerning the decay of the vortex body. The flow of energy between the different scales is then visualised by filtering the Navier-Stokes equation and qualitatively shown to be non-isotropic with respect to the vortex core.

## Introduction

Although the scientific observation of what today constitutes fluid mechanics can be dated at least to 250 BC with Archimedes, the origin of the word *turbulence* referring to a chaotic water flow (originating from the latin *turba*: chaos, disorder) has to be traced back to 1507: this term is another invention of Leonardo da Vinci himself, (see [1], [2]), who dedicated considerable time and efforts to the study of this topic and produced astonishing representations of eddying and whirling motions in water.



FIG. 1: One of the most famous representations of turbulent flow by Leonardo da Vinci

To find a proper starting point for our discussion we move forward to the work of Kraichnan [3], Leith [4], and Batchelor [5], which introduce one of the peculiarities of turbulence in two dimensions - the so called **inverse energy cascade** (See the plot of  $E(k)$  in Figure 2a): the energy introduced in the system at a certain length scale tends to flow towards larger scales of motion (Figure 2b), and this process characterises two-dimensional turbulence only, as in three dimensions energy flows instead towards small scales where it gets dissipated (*direct energy cascade*). For the intermediate scales, the so called *inertial range*, the slope of the  $E(k)$  plot / exponent  $\gamma$  of  $E(k) \propto k^\gamma$  as in Figure 2a is  $-\frac{5}{3}$ , as Kolmogorov has elegantly proved in [6] in 1941 by means of dimensional analysis only.//

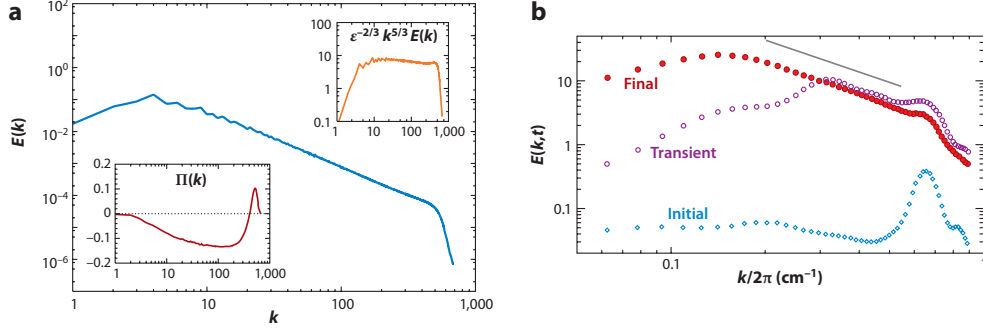


FIG. 2: The inverse cascade, energy  $E$  over wavenumber  $k$  (a) and its evolution (b) (from [7])

The phenomenon of the inverse energy cascade, caused by a nonlinear coupling between different scales of motion in the Navier-Stokes equations, takes place until a limit size, imposed by the finite boundaries of the systems, is reached. Energy then "piles up" in coherent structures, namely a positive/negative vortex dipole: Figure 3 shows how the system evolves towards this configuration as the smaller structures are washed out and absorbed into the two main vortices. The main subjects of this report are the shape of these vortices formed as the previously mentioned phenomenon of inverse energy cascade takes place, and the energy flow from one scale size to another: we initially analyse a numerical simulation of turbulence and compare the structural properties of vortices with the currently accepted (although more and more discussed) hypothesis of a velocity profile  $V(r) \propto r^{-\frac{1}{4}}$  (please notice how this is equivalent to the vorticity profile  $\omega(r) \propto r^{-\frac{5}{4}}$  considered from now onwards). Using the same model we then focus on the energy flow from one scale to the other and its asymmetry towards smaller scales that origins the inverse energy cascade.

This miniproject was originally intended to retrace and verify numerically the calculations and assumptions in [8], where the  $-\frac{1}{4}$  scaling exponent for the velocity within a vortex is proven to be right (and claimed to be universal, as in not related to the geometry of the box or details of the forcing acting on the system) by purely theoretical means, but the side-quests emerged during this process proved to be of no less relevance and interest, although more feasible in the limited time in which this research was expected to be completed, and have therefore become the main topic of discussion [17].

### The Navier-Stokes Equations

It is worth explaining briefly the structure of these fundamental equations of fluid dynamics, somehow the direct extension of Newton's Laws to fluids. In their most general form, they are:

$$\begin{cases} \rho \left( \frac{\partial \vec{v}}{\partial t} + \vec{v} \cdot \nabla \vec{v} \right) = -\nabla p + \nabla \cdot \mathbf{T} + \vec{F} & \text{conservation of momentum} \\ \frac{\partial \rho}{\partial t} + \nabla \cdot (\rho \vec{v}) = 0 & \text{conservation of mass} \end{cases}$$

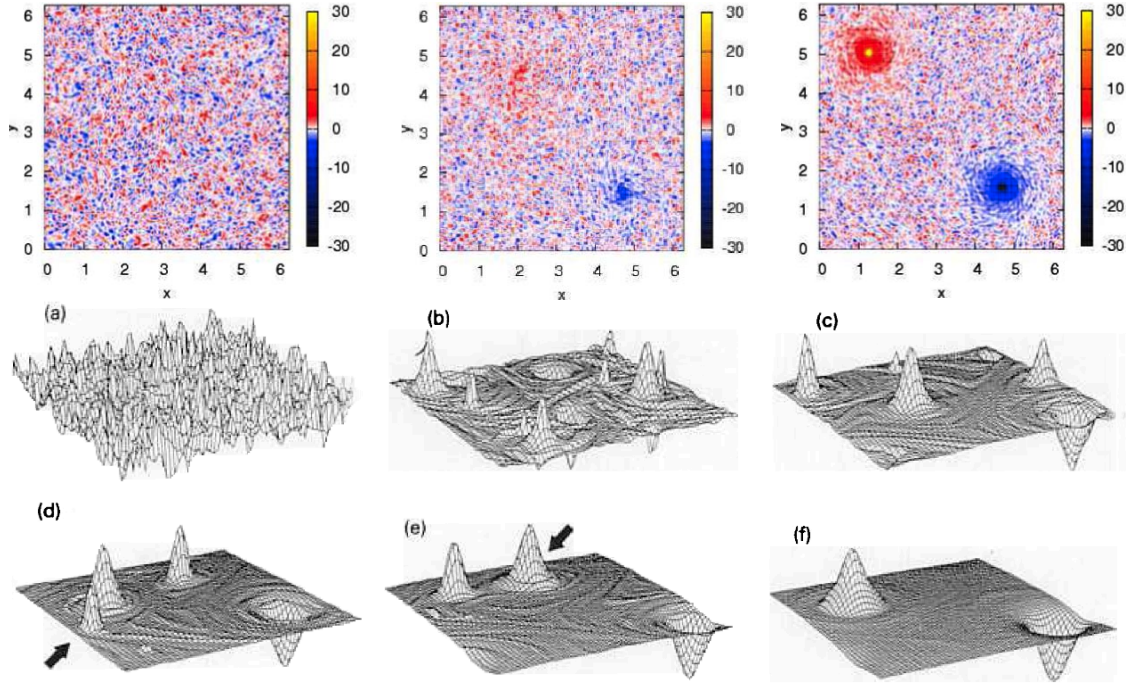


FIG. 3: The vortices dipole emerges from a disordered configuration (top: from [9], bottom: from [10])

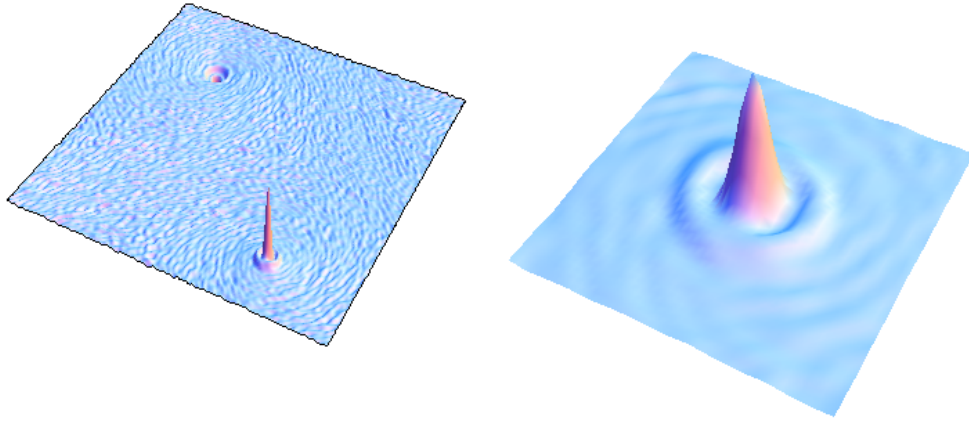


FIG. 4: Single snapshot of the system (vorticity field over  $[0, 2\pi]^2$ ) and zoom on the positive vortex

and can be simplified for the incompressible case as

$$\begin{cases} \rho \left( \frac{\partial \vec{v}}{\partial t} + \vec{v} \cdot \nabla \vec{v} \right) = -\nabla p + \mu \nabla^2 \vec{v} + \vec{F} \\ \frac{\partial \rho}{\partial t} + \nabla \cdot (\rho \vec{v}) = 0 \end{cases}$$

where  $\rho$  is the fluid density,  $\vec{v}$  is the flow velocity,  $p$  is the pressure,  $\mathbf{T}$  is the stress tensor,  $\vec{F}$  is the resultant of the forces acting on the fluid per unit of mass (or *body forces*) and  $\mu$  is the

dynamic viscosity. Further equations may include informations about the boundary conditions, other conservations (we assumed the conservation of mass, but this is not necessarily true) or more.

We will consider the case of an incompressible fluid and generally mention the equation for the conservation of momentum as "the" Navier-Stokes equation. In the following representation, the role of each of its terms is mentioned [18]. (For a deeper discussion on the topic one can refer to any good manual on fluid dynamics, as [11])

$$\rho \left( \underbrace{\frac{\partial \mathbf{v}}{\partial t}}_{\text{Unsteady acceleration}} + \underbrace{\mathbf{v} \cdot \nabla \mathbf{v}}_{\text{Convective acceleration}} \right) = \underbrace{-\nabla p}_{\text{Pressure gradient}} + \underbrace{\mu \nabla^2 \mathbf{v}}_{\text{Viscosity}} + \underbrace{\vec{F}}_{\text{Other body forces}}.$$

It has to be evidenced the relevance of  $\mathbf{v} \cdot \nabla \mathbf{v}$ : this is the part making the whole equation nonlinear, and therefore unsolvable/extremely interesting.

## I. DATA ANALYSIS

The model (the very same used in [9]) generates our system in a  $[0, 2\pi] \times [0, 2\pi]$  box ( $256^2$  gridpoints) with periodic boundary conditions. For a bidimensional flow, vorticity can be represented as a scalar field  $[0, 2\pi] \times [0, 2\pi] \rightarrow \mathbb{R}$ , since  $\nabla \times (u_x, u_y, 0) = (0, 0, \omega_z)$ . Once the initial transient has finished and the dipole has been formed, the system looks like Figure 4: the two vortices are evident, and it is possible to observe a certain pattern surrounding them. 100 of such snapshots of the vorticity field were provided for the data analysis.

The first task is to centre the (positive) vortex, as this eliminates finite-size issues when evaluating the distances of every point from this vortex, making it straightforward as it is not required to take into account the boundary conditions. The values of  $\omega(r, \theta)$  are then averaged over the angle and then over all the snapshots in order to obtain an averaged vorticity profile only depending on the radius, as shown in Figure 6. We expect to distinguish three different regions within a vortex: a **core**, for  $r <$  forcing scale, a **tail**, in which the interactions with the opposite vortex start to become relevant, for  $r > \frac{1}{4}$  of the box size, and a main **body** in between. In our case the cutoff in the vorticity profile between body and tail is actually present at  $r$  values smaller than  $\frac{1}{4}$ , and this will become crucial soon.

The averaged vorticity profile obtained is also compared to one obtained from an "ideal vortex dipole" in Figure 7 (how to obtain such an ideal profile, implementing the boundary conditions, is explained in Appendix A): it is interesting to notice how this actually presents the cutoff at  $\frac{\pi}{2}$  as just mentioned, while the "real" system seems to exhibit an earlier cutoff at approximately  $\frac{\pi}{4}$ .

The range over which the exponent has to be fitted must be chosen in order to exclude the core and the tail: for our generating model we know the forcing scale to be about  $\frac{1}{50}$  of the box, which gives

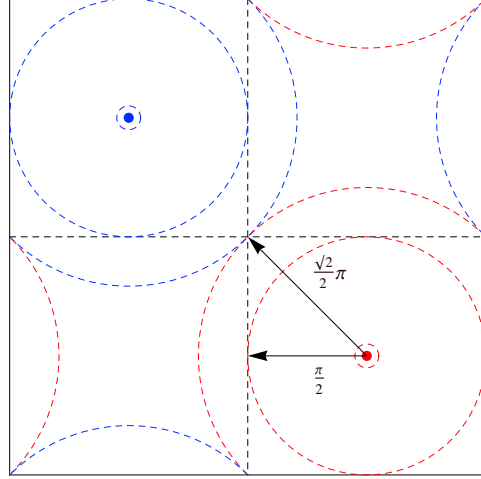


FIG. 5: Ideal position of two vortices in the  $[0, 2\pi]$  box plus periodic boundaries, and some significant distance related to their interaction (red and blue indicate positive and negative vortex)

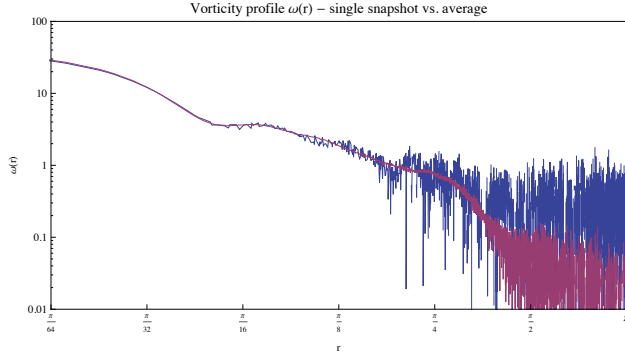


FIG. 6: Vorticity profile - single snapshot vs. average

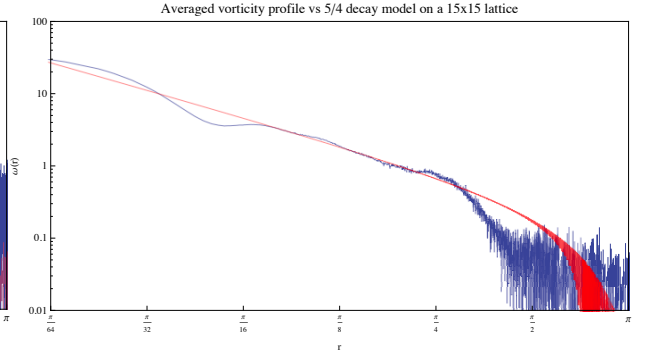


FIG. 7: Average vs ideal vortex dipole

us a lower bound of  $r_{min} = \frac{2}{50}\pi$ ; on the other end we want to consider that part of system which is influenced by a single vortex and therefore we may want to stop at some point between  $r_{max} = \frac{1}{2}\pi$  and  $\frac{1}{4}\pi$  - we will, for now, consider these two extreme values as the right boundary of our region of interest. By fitting our exponential function in these two regions,  $[\frac{2}{50}\pi, \frac{1}{4}\pi]$  and  $[\frac{2}{50}\pi, \frac{1}{2}\pi]$  for each snapshot we obtain 100 values of the (two) exponents, which averages are comparable to the exponents found by directly fitting the averaged vorticity profile within the same regions, but in this way it is also possible to obtain an uncertainty on these measures. Figure 9 shows the fitting functions  $\omega(r) \propto r^\alpha$  as obtained over the range  $[\frac{1}{25}\pi < r < \frac{1}{4}\pi]$  in magenta,  $[\frac{1}{25} < r < \frac{1}{2}\pi]$  in red, and plotted together with the  $-\frac{5}{4}$  slope (in black, dashed): the uncertainty on these  $\alpha$  is also present as error bars, and the histograms in Figure 8 show how the values of  $\alpha$  are distributed.

The obtained values of  $\alpha$ ,  $\alpha_1 = -1.07 \pm 0.02$  and  $\alpha_2 = -1.304 \pm 0.015$  seem directly incompatible with  $\alpha = -1.25$ , but it has to be stressed that the choice of which region to fit (specifically, of the boundary between the body and the tail of the vortex) has not been done in a rigorous way. One can in fact turn this problem upside down by looking at the form of the velocity profile,

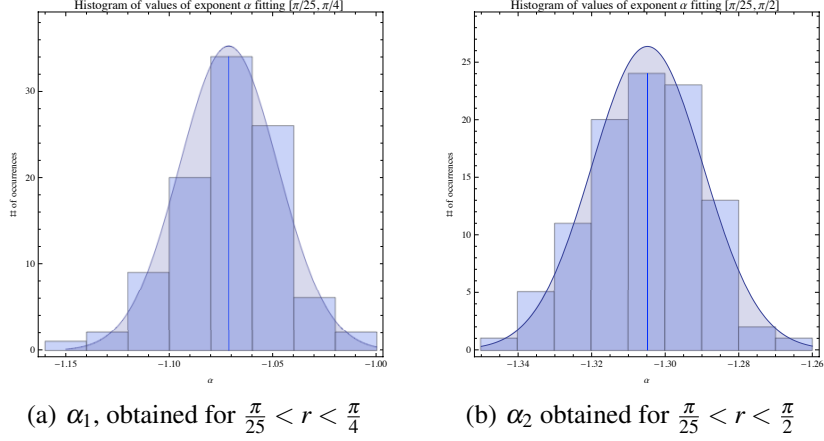


FIG. 8: Distribution of  $\alpha$  from fit on single snapshots: superimposed, Gaussians with same  $\mu$  and  $\sigma$

especially between the values  $\frac{\pi}{4}$  and  $\frac{\pi}{2}$ , and considering that for the first the fitting exponent is too high, while for the second it is too low: for a question of continuity we should be able to determine a new  $r_{max}$  somewhere in between those two values such that the fitted exponent is (almost) anything in between  $\alpha_1$  and  $\alpha_2$ , and so we can find a good region to fit  $-\frac{4}{5}$  [19] for  $r_{max} \approx \frac{3}{7}\pi \approx \frac{4}{3}$ .

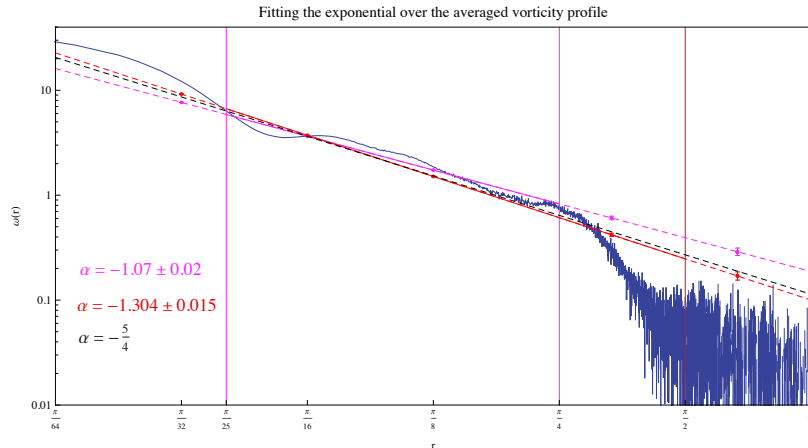


FIG. 9: Fitting exponents for  $[\frac{\pi}{25}, \frac{\pi}{2}]$  and  $[\frac{\pi}{25}, \frac{\pi}{4}]$  (in red and magenta, respectively)

## II. FILTERED NS

Given a certain function  $f(\vec{x})$ , we define its filtered version according to the filtering scale  $\ell$  as

$$\bar{f}_\ell(\vec{x}) = \int d\vec{y} f(\vec{y}) G_\ell(\vec{x} - \vec{y})$$

where  $G_\ell(\vec{x}) = G\left(\frac{1}{\ell^d}\vec{x}\right)$ ,  $G(\vec{x})$  is our filtering distribution - for us, a Gaussian  $\frac{1}{\sqrt{2\pi}}e^{-\frac{x^2}{2}}$ , and  $d$  is the dimensionality of  $\vec{y}$ .

It is important to notice that the filtering operator is linear and commutes with the differentiation, as in  $\partial_x \bar{f}_\ell = \overline{(\partial_x f)}_\ell$ , and this will be of great use when dealing with the filtering of Navier-Stokes equations.

This gaussian filtering operates a smoothening of the function on which it is applied, and the larger the  $\ell$  the stronger its effect, as it is shown in Figure 11: this smoothening can be seen somehow as a blurring of the field, for which each point will adjust its value according to his neighbours, weighting them with  $G_\ell(\vec{x})$ . It is easy to see its effect on an image, as in Figure 10:

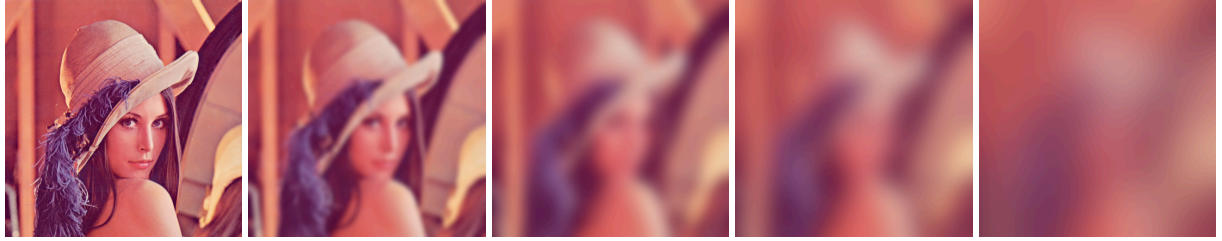


FIG. 10: The effects of Gaussian filtering on an image: original and  $\ell = 5, 15, 25, 50$  pixels

Similarly, acting on a scalar field, it smoothenes it out progressively:

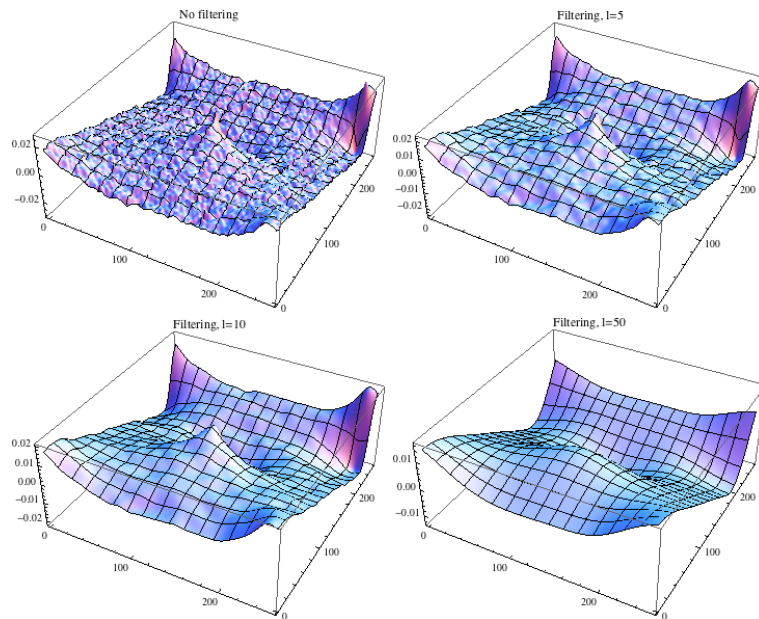


FIG. 11: An original function and three different filterings at  $\ell = 5, 10, 50$

The previously shown Navier-Stokes equation (conservation of momentum) with no body forces can be written, according to Einstein notation, as

$$\partial_i u_i + (u_j \partial_j) u_i = -\partial_i p + \nu \partial_{ii} u_i$$

By noticing that  $\partial_i u_i = 0$  is the new notation equivalent of  $\nabla \cdot \vec{u} = 0$ , which is true due to the incompressible assumption, we can see how  $\partial_j (u_j u_i) = u_j (\partial_j u_i) + \cancel{(\partial_j u_j) u_i} = u_j (\partial_j u_i)$  and rewrite the whole equation as

$$\partial_t u_i + \partial_j (u_i u_j) + \partial_i p - \nu \partial_{ii} u_i = 0$$

before applying the filter (remember the previously mentioned properties of linearity and commutation with the differentiation operator) [20]

$$\overline{\partial_t u_i + \partial_j (u_i u_j) + \partial_i p - \nu \partial_{ii} u_i} = 0 \quad \rightarrow \quad \partial_t \bar{u}_i + \partial_j (\bar{u}_i \bar{u}_j) = -\partial_i \bar{p} + \nu \partial_{ii} \bar{u}_i$$

The filtering acts therefore on each component of the equation individually, and it is by easy algebra that we obtain what follows

$$\begin{aligned} \partial_t \bar{u}_i + \partial_j (\bar{u}_i \bar{u}_j) &= -\partial_i \bar{p} + \nu \partial_{ii} \bar{u}_i \\ \partial_t \bar{u}_i + \partial_j (\tau_{ij} + \bar{u}_i \bar{u}_j) &= -\partial_i \bar{p} + \nu \partial_{ii} \bar{u}_i \quad (\text{having defined } \tau_{ij} = \bar{u}_i \bar{u}_j - \bar{u}_i \bar{u}_j) \\ \partial_t \bar{u}_i + \partial_j (\bar{u}_i \bar{u}_j) + \partial_i \bar{p} - \nu \partial_{ii} \bar{u}_i &= -\partial_j \tau_{ij} \\ \Rightarrow \text{Filtered Navier-Stokes} &= \text{Navier-Stokes} + \partial_j \tau_{ij} \end{aligned}$$

By filtering the Navier-Stokes equations we therefore obtain a new term,  $\partial_j \tau_{ij}$ , which will act either as a source or sink given by the interaction at smaller scales ( $< \ell$  used for filtering). This  $\tau_{ij}$  is the turbulent stress tensor, a sort of measure of the correlation between filtered velocities given by  $\tau_{ij} = \bar{u}_i \bar{u}_j - \bar{u}_i \bar{u}_j$

In analogy to the classic kinetic energy  $K = \frac{1}{2} m v^2$  we define the *large scale kinetic energy* as  $e = \frac{1}{2} \bar{u}_i \bar{u}_i$ . From a straightforward differentiation of this quantity, and using the same  $\partial_t \bar{u}_i$  from the filtered Navier-Stokes above, we obtain:

$$\partial_t e = \bar{u}_i \partial_t \bar{u}_i = -\bar{u}_i \partial_j (\bar{u}_i \bar{u}_j) - \bar{u}_i \partial_i \bar{p} + \bar{u}_i \nu \partial_{ii} \bar{u}_i - \bar{u}_i \partial_j \tau_{ij}$$

A certain number of equalities, some quite obvious, some less, allows us to obtain from this expression a continuity equation of the form

$$\partial_t e + \partial_i J_i = -\nu (\partial_i \bar{u}_i)^2 + \Pi \quad (1)$$

where  $J_i$  is the spatial flux of the large scale energy and  $\Pi = \Pi(x, y)$ , with its dimension of  $[\text{energy} \cdot \text{time}^{-1}]$ , is the term describing the scale-to-scale energy flux that we will be considering. This  $\Pi(x, y)$  has been obtained numerically from 100 snapshots of the stream function  $\psi$  over  $[0, 2\pi]^2$ : its shape within the box can be seen in Figure 13, while a plot of different values of  $\Pi_{tot} = \sum_{(x, y) \in [0, 2\pi]^2}$  for different snapshots is shown in Figure 12. It is worth noticing how  $\Pi$  is *not* isotropic on the vortex, as the vorticity was instead (compare Figure 4, right, and Figure 13, right).

An easier way to visualise the geometry (and non-isotropy) of this energy flow is to use contour plots, as in Figure 14 (a different snapshot has been considered). From these it is possible to notice that my work has a major flaw: periodic boundary conditions were *not* implemented for this part of work, as once the previous analysis was completed without them they proved to be computationally too demanding for giving any result in a short time, and a brief discussion of how this lack has influenced the results is presented in Appendix B. A

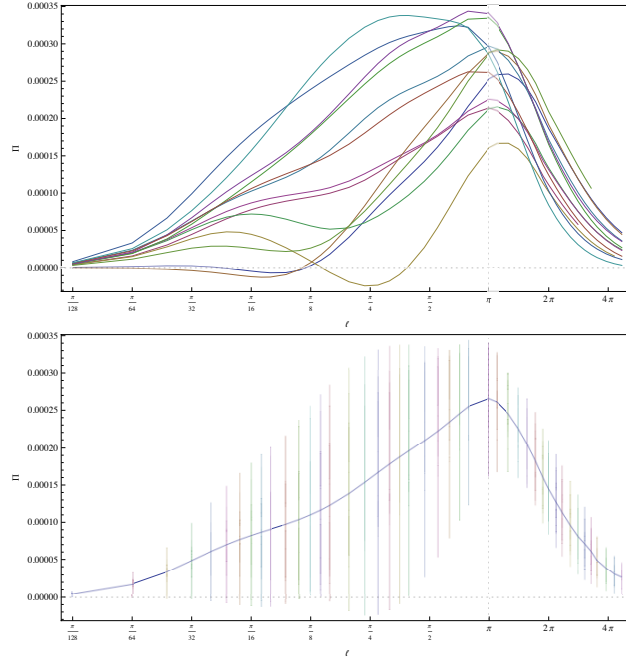


FIG. 12: (top) Values of  $\Pi$  (summed on the whole box) for different  $\ell$ . Each line is a snapshot. (bottom)  $\Pi$  averaged on the different snapshots: the vertical bars are the range of  $\Pi$  for those values of  $\ell$ .

better algorithm for solving this issue would be an ideal (and necessary) continuation to this report.

From Figure 12 we see how the term  $\Pi_{tot}$  is mostly positive, confirming a flux of energy towards the small scales, although for some lines=snapshots the system actually brings some energy back to *smaller* scales. The dependance of the averaged  $\Pi_{tot}$  on  $\ell$  is furthermore a topic on which I would like to continue working, both for understanding how the lack of boundary conditions in our case has compromised the result and also to find any explicit relation  $\Pi_{tot} = f(\ell)$ .

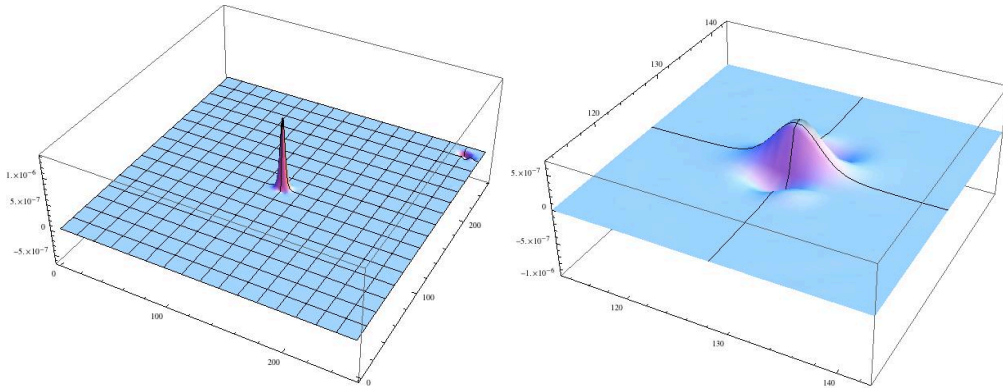


FIG. 13: Plot of  $\Pi(\vec{x})$  and closeup on the central (positive) vortex

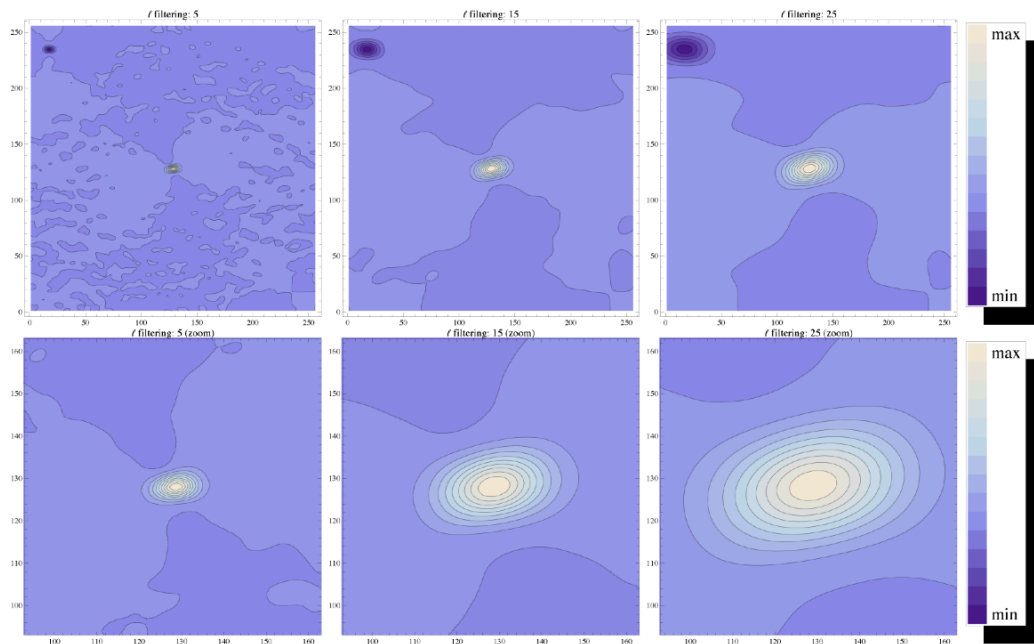


FIG. 14: Contour plots of  $\Pi(x,y)$  and closeup on the central vortex (approx.  $[0.75\pi, 1.25\pi]^2$ ). Filtering lengths:  $\ell = 5, 15, 25$ . The range of values (min/max reported in the legend on the right) may vary severely according to different snapshots and different  $\ell$ s up to  $\Pi(x,y) \pm 10^{-6} J/s$  (calculated on a single gridpoint)

### III. CONCLUSIONS AND FURTHER WORK

In conclusion, it is certainly interesting the fact that data analysis seems to contradict the current model of  $V(r) \propto r^{-\frac{1}{4}}$  if we consider, as the limit between body and tail of a vortex, two of the values that appear to be the most sensible. The question becomes then: *why* should we consider a  $r_{max} \approx \frac{3}{7}\pi$  to be the correct value of such boundary? Are there physical considerations that may justify this? If these are lacking, then one may actually seriously consider whether the current model is correct.

As for the energy flux, it is shown how this is related to the filtering length  $\ell$ , but the missing boundary conditions have a growing relevance effecting the results as this value increases. The spatial dependence of the energy flow process is nevertheless validly represented for small  $\ell$ s and probably not too dissimilar from the actual behaviour. On this part of the work the unsolved questions are many, starting from the previously mentioned dependence of the averaged  $\Pi_{tot}$  on  $\ell$ , to finding a better algorithm for processing the filtering and analysis, to the role of boundary conditions.

### Appendix A: A model of vortex dipole and the implementation of boundary conditions

It is interesting to try and build an ideal vorticity field which profile decays exactly as  $-\frac{5}{4}$  in order to directly visualise how the analysed system differs from it. Given the positive vortex to be centred in  $(x_+, y_+)$  and the negative one similarly in  $(x_-, y_-)$ , we define this field as

$$f(x, y) = \frac{1}{\sqrt{(x-x_+)^2 + (y-y_+)^2}^{\frac{5}{4}}} - \frac{1}{\sqrt{(x-x_-)^2 + (y-y_-)^2}^{\frac{5}{4}}} = d_+(x, y)^{-5/4} - d_-(x, y)^{-5/4} \quad (\text{A1})$$

where  $d_+$  and  $d_-$  are the distances of a given point from the positive and negative vortex. This function is easily evaluated  $\forall \vec{x} = (x, y) \in \mathbb{R}^2 / \{\vec{x}_-, \vec{x}_+\}$  (where  $\vec{x}_-$  and  $\vec{x}_+$  are the positions of the two vortices, on which the function would have a singularity), but we are interested in applying it to our *finite* case  $[0, 2\pi]^2$  with periodic boundary conditions. There are two equivalent ways to implement these:

- first, we may extend our region of interest from one box to  $n \times n$  boxes: assume that our original box was  $[-\pi, \pi]^2$  (shifted for simplicity), we now consider  $[-(2n+1)\pi, (2n+1)\pi]^2$ , but leave the vortices where they originally were - we simply drop our boundaries and evaluate the function further away from  $\vec{x}_-, \vec{x}_+$ . Once we obtained  $f(\vec{x})$  as previously defined within this larger region, we say that

$$\tilde{f}(x, y) = \sum_{i, j=-n}^n f((2i+1)x, (2j+1)y)$$

which intuitively means that, once  $f$  has been calculated for every point in the extended region, all the copies of the original  $[-\pi, \pi]^2$  box are superimposed and the value of  $\tilde{f}(x, y)$  is given by the sum of  $f(x, y)$  of the  $n$  superimposed points.

- alternatively, we may work in the "opposite" way: instead of keeping the vortices fixed and extend our measurements far over the boundaries, we can create "virtual" copies of our vortices outside the main box, as in a (finite) lattice  $\Lambda$ , and then, picked a point within the box, evaluate *all* the distances from  $(\vec{x}_-)_i, (\vec{x}_+)_j, i, j \in \Lambda$  (all the vortices forming the lattice).

We end up with a formula which generalises equation (A1) for more than two vortices, as

$$f(x, y) = \sum_{i \in \Lambda} \frac{\text{sign}(\Lambda_i)}{\sqrt{(x-x_{\Lambda_i})^2 + (y-y_{\Lambda_i})^2}^{\frac{5}{4}}} = \sum_{i \in \Lambda} \text{sign}(\Lambda_i) d(x_{\Lambda_i}, y_{\Lambda_i})^{-\frac{5}{4}} \quad (\text{A2})$$

where  $\Lambda_i$  refers to the  $i$ -th vortex on the lattice, which coordinates are  $(x_{\Lambda_i}, y_{\Lambda_i})$ . This equation is actually a particular case of Weierstrass'  $\wp$ -function

This second method proved easier to implement and was used to generate different pseudo-vorticity profiles: in Figure 15 we can see how these evolve as the lattice gets bigger and bigger - at  $15 \times 15$  the profile looks already stabilised and the cutoff starting at  $\frac{\pi}{2}$  discussed

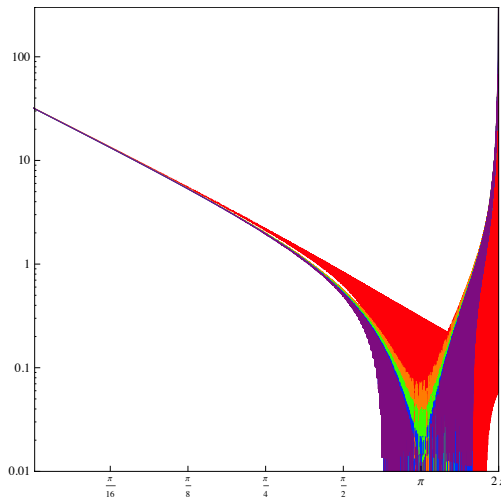


FIG. 15: pseudo-vorticity profiles using (A2) on different lattice sizes (from  $1 \times 1$ , red, to  $15 \times 15$ , purple)

### Appendix B: Lack of Periodic Boundary Conditions in Gaussian Filtering

Due to computational reasons, it has not been possible to perform the analysis of section II with the requested periodic boundary conditions, as shown from the contour plots of Figure 11 that exhibit no continuity between the left/right and top/bottom edge. This means that points within a distance  $d < \ell$  from the boundaries will not see a certain number of points on the other side/s during the filtering, but also,  $\forall \ell < 128 (\ell < \pi \text{ in the correct notation}), \exists \mathcal{S} \subset [0, 2\pi]^2$  in which the filtering is correct, and having centred the positive vortex means that its shape, as shown in Figure 11 actually is the feature that remains correct for the highest values of  $\ell$ , while on the boundaries of the boxes it is almost immediately noticeable how this mistake is relevant. What is even more important is how this could have affected the results shown in Figure 12: is the behaviour exhibited for large  $\ell$  still valid?

### Acknowledgements

My most sincere thanks are for my project supervisor, Colm Connaughton, to be praised for his patience and thanked for all that he has taught me during these months. Working with him has been greatly motivating, and I hope he will find my results satisfactory and may possibly be willing to use my help to continue this research in the future.

I also thank Guido Boffetta for the precious (and reasonably pessimistic) chat we had at the beginning of this project, and in the hope that the department of Complex Systems of my alma mater University of Torino and the Centre for Complexity Science may begin soon some mutually useful interaction, and Gareth Alexander for his suggestions about the lattice problem analysed in Appendix A.

## Bibliography

---

- [1] M.R.C. Bell and J.P. Richter. *The notebooks of Leonardo da Vinci*, volume 2. Dover Pubns, 1970.
- [2] R. Ecke. The turbulence problem. *An Experimentalist Perspective (Los Alamos Science, Number 29, 2005)*, 2005.
- [3] R.H. Kraichnan. Inertial ranges in two-dimensional turbulence. *Physics of Fluids*, 10:1417, 1967.
- [4] CE Leith. Diffusion approximation for two-dimensional turbulence. *Physics of Fluids*, 11:671–672, 1968.
- [5] G.K. Batchelor. Phys. fluids suppl. 12, ii-233 (1969); r. kraichnan. *Phys. Fluids*, 10:1417, 1967.
- [6] A. Kolmogorov. The local structure of turbulence in incompressible viscous fluid for very large reynolds' numbers. In *Akademiia Nauk SSSR Doklady*, volume 30, pages 301–305, 1941.
- [7] G. Boffetta and R.E. Ecke. Two-dimensional turbulence. *Annual Review of Fluid Mechanics*, 44(1), 2012.
- [8] M. Chertkov, I. Kolokolov, and V. Lebedev. Universal velocity profile for coherent vortices in two-dimensional turbulence. *Physical Review E*, 81(1):015302, 2010.
- [9] M. Chertkov, C. Connaughton, I. Kolokolov, and V. Lebedev. Dynamics of energy condensation in two-dimensional turbulence. *Physical review letters*, 99(8):84501, 2007.
- [10] WH Matthaeus, WT Stribling, D. Martinez, S. Oughton, and D. Montgomery. Decaying, two-dimensional, navier-stokes turbulence at very long times. *Physica D: Nonlinear Phenomena*, 51(1):531–538, 1991.
- [11] D.J. Tritton. *Physical fluid dynamics*, volume 1. 1988.
- [12] R.H. Kraichnan and D. Montgomery. Two-dimensional turbulence. *Reports on Progress in Physics*, 43:547, 1980.
- [13] P. Tabeling. Two-dimensional turbulence: a physicist approach. *Physics reports*, 362(1):1–62, 2002.
- [14] S. Chen, R.E. Ecke, G.L. Eyink, M. Rivera, M. Wan, and Z. Xiao. Physical mechanism of the two-dimensional inverse energy cascade. *Physical review letters*, 96(8):84502, 2006.
- [15] G. Boffetta. Energy and enstrophy fluxes in the double cascade of two-dimensional turbulence. *Journal of Fluid Mechanics*, 589:253–260, 2007.
- [16] Z. Xiao, M. Wan, S. Chen, and GL Eyink. Physical mechanism of the inverse energy cascade of two-dimensional turbulence: a numerical investigation. *Journal of Fluid Mechanics*, 619:1, 2010.
- [17] Nevertheless, although not reported here, the completed steps of retracing the calculations have been an interesting exercise in differential geometry, fluid dynamics and operator theory in PDEs.
- [18] Creative Commons Attribution-ShareAlike - modified from en.wikipedia.com, "Navier-Stokes equations"
- [19] We should discuss how close to  $-\frac{4}{5}$  can an exponent found with this method be - since we are fitting over a finite number of points, it is impossible to fine-tune our fitting interval in such a way to obtain a result *arbitrarily* close to a particular value. Anyways, since there is a finite uncertainty on our result, we can expect to obtain an exponent which results totally compatible with the expected  $-\frac{4}{5}$
- [20] notice that all the filtered quantities should specify the  $\ell$ , as in  $(\bar{u}_j)_\ell$ , but we will drop it from our notation unless strongly required